

Optimized breath detection algorithm in Electrical Impedance Tomography

D. Khodadad¹, S. Nordebo¹, B. Muller, A. Waldman, R. Yerworth, T. Becher, I. Frerichs, L. Sophocleous, A. Van Kaam, M. Miedema, M. Kallio, N. Seifnaraghi², R Bayford.

¹ Department of Physics and Electrical Engineering, Linnaeus University, 351 95 Växjö, Sweden

² Department of ...

E-mail: davood.khodadad@lnu.se

Abstract.

Objective: This paper gives a general framework for optimizing the breath delineation algorithms used in Electrical Impedance Tomography (EIT). In lung EIT the delineation of the breath phases is central for generating tidal images, subsequent data analysis and clinical evaluations. The optimization of these algorithms is particularly important in neonatal care since existing breath-detectors developed for adults may give insufficient reliability due to the very irregular breathing patterns obtained with neonates in comparison to adults. *Approach:* The approach is generic in the sense that it relies on the definition of a gold standard and the associated definition of detector sensitivity and specificity, an optimization criterion and a set of detector parameters to be investigated. The approach is illustrated here with an example based on a small dataset and a gold standard defined by 11 EIT experienced clinicians within the EU-funded CRADL project. *Main results:* Three different algorithms are proposed that are improving the breath detector performance by adding conditions on 1) maximum of tidal breath rate obtained from zero-crossings of the breathing signal, 2) minimum of tidal amplitudes and 3) minimum of tidal breath rate obtained from Time-Frequency (TF) analysis (apnea alarm). *Significance:* Based on the gold standard, the most crucial parameters of the proposed algorithms are optimized by using a simple exhaustive search and a weighted metric defined in connection with the Receiver Operating Characteristics (ROC). This provides a practical way to achieve any desirable trade off between the sensitivity and the specificity of the detectors.

Keywords: EIT, breath detection, respiratory system, optimization, lung imaging, ROC, inspiration, expiration.

1. Introduction

Robust and reliable detection and delineation of breaths known as a breath detection is the basis of lung functionality analysis. The aim of the breath detector is to obtain information about the exact timing of the two respiration phases: inspiration and expiration. Accurate breath detection is a key parameter in respiratory related clinical use which has multiple applied and cross-disciplinary applications. However, this process is technically challenging due to the noisy nature of the acquired data obtained from the thorax area, measurement artifacts and other factors such as the presence of sighs, swallows, transient reductions and pauses (hypopneas and apneas) in

breathing. In order to quantify key breathing parameters, accurate identification of inspiration and expiration phases in each breath cycle is required.

Different methods to quantify respiration have been attempted during the last years. Measuring airflow pressure, volume signal, or both are examples of the traditional methods which need a breathing mask [1, 2]. For example, airway flow curves are used as the basic delineator while the airway pressure and the CO₂ concentration curves are used to confirm the delineation [3]. However, the method is time consuming and potentially prone to human error and indeed impractical for large data sets. In order to cope with these problems, automated physiological landmark detection in the airflow or epiglottis pressure signal (Pepi) methods are introduced [4]. However, the presence of baseline volume shifts, can still render these algorithms inaccurate.

Similar to the breath airflow methods, breath sound detection algorithms are also developed to detect the breath cycle. Although these methods are used in clinical practice, they are mostly developed for industrial applications such as breath sound removal/suppression in the music industry and monitoring firefighters' respiration during their duties. These methods are based on a template matching approach, and therefore, they are more reliable for adult normal breath detection [5]. Recently, transcutaneous electromyography of the diaphragm (dEMG) is used for non-invasive breath detection based on the measurement of electrical activity of the diaphragm [6, 7].

Electrical impedance tomography (EIT) is a non-invasive bedside tool in which impedance or voltage changes are present due to changes in the regional ventilation. In addition, it allows monitoring the functionality of the lungs. Computerized Tomography (CT) and Magnetic Resonance Imaging (MRI) could achieve this goal but not at the bedside. Online X-ray monitoring may increase the risk of increased ionization due to the need for successive imaging. Further, these modalities are incompatible with the neonatal application as they demand full cooperation with the patient to be stable, which is not feasible [7-10]. Furthermore, CT and MRI do not produce dynamic images and it is not possible to achieve continuous monitoring of regional lung ventilation in Neonatal Intensive Care Unit (NICU). However, unlike CT or other radiographic techniques, EIT is an inexpensive technology which makes continuous real-time radiation free monitoring of the lung function possible directly at the bedside without any known hazard. The EIT therefore can be an ideal candidate to be applied for monitoring mechanically supported neonates [8-14].

The main scope of this study is to provide a general approach to achieve an optimized breath delineation for neonates and premature newborns using an EIT device. A significant number of studies for lung function monitoring using EIT have been published in recent years [15-19]. There are different methods to resolve the respiratory related information from the chest EIT signal. Peak and slope detection based on the breathing (impedance) signal is straightforward in order to determine the breathing cycles in tidal breathing [4, 5, 20]. Indeed, the slope of the breathing signal shows whether the total impedance is increasing or decreasing in order to determine the inspiration and expiration phases. However, due to the presence of cardiac related signal components and other disturbances, the method is prone to yield high error rates. Frequency domain filtering is attempted as a solution to decompose and extract cardiac and respiratory related signals [16, 21, 22]. However, the method often suffers from a frequency overlap of the respiration harmonics and the heartbeat signal. In order to achieve a proper separation of the respiratory and cardiac-related signals, Principal Component Analysis (PCA) may be used. The PCA demands identification of template functions for time domain filtering. It is a multivariate statistical method and also time consuming which makes the method not suitable

for real time analysis [17]. Consequently, Independent Component Analysis (ICA) has been used to increase the accuracy of decomposing the EIT signal into independent components based on statistical characteristics of the signals [23].

In our study, the following algorithms are proposed (in the order of increased complexity)

- 1) the zero-crossing (ZC) algorithm,
- 2) the zero-crossing algorithm with amplitude threshold (ZC-AT),
- 3) the zero-crossing algorithm with amplitude threshold and FFT-based breath rate estimation (ZC-AT-FFT).

The algorithms are using as input the total impedance signal obtained from EIT and are improving the detector performance by adding conditions on 1) maximum of tidal breath rate obtained from zero-crossings of the breathing signal, 2) minimum of tidal amplitudes and 3) minimum of tidal breath rate obtained from Time-Frequency (TF) analysis (apnea alarm). In analogy to [5, 20] we determine the breathing cycle from the position of peaks and slopes in the breathing signal and add an extra criteria regarding the minimum distance in between zero crossings at one half and a full cycle, respectively. In this way, higher oscillating error sources are avoided. In the second algorithm, an amplitude threshold is used to remove small amplitude fluctuations (e.g., cardiac related) which are not breaths. Finally, in the third algorithm, the Short-Time Fourier Transform (STFT) is employed to dynamically estimate the breath rate, facilitating a lower bound on what is realistically considered to be a breath (e.g., by detecting hypopneas and apneas) [24].

The most crucial parameters of these algorithms are optimized by using a simple exhaustive search and a weighted metric defined in connection with the Receiver Operating Characteristics (ROC). This provides a practical way to achieve any desirable trade-off between the sensitivity and the specificity of the detectors. The approach is generic and is illustrated here with an example based on a small dataset with clinical EIT data from an ongoing study within the EU-funded [CRADL](#) project. A gold standard was defined based on 80 % certainty (agreement) where 11 EIT experienced clinicians were asked to examine the corresponding impedance plots and to define the corresponding breath phases. It is emphasized that this approach is non-parametric in the sense that no statistical assumptions have been made on the population distributions from which the data are drawn. To this end, the non-parametric gold standard constitutes a generic approach which is currently under development and is expected to be useful in many other EIT related issues and investigations where breath delineation and tidal breathing is of great importance, see e.g., [25].

2. Methods

2.1. Data acquisition

Data collection is performed in a prospective study comprising 10 pediatric patients as part of the CRADL project. The study is approved and funded by EU as Continuous Regional Analysis Device for neonate Lung (CRADL) project under the ethic ID number of NCT02962505. The raw EIT data are acquired by the Swisstom EIT belt system with 32 electrodes at the frame rate of 48 Hz. This system is specially designed for infants who had thorax diameters as small as 17.5 cm. Current injections with amplitude of 3 mA rms at a frequency of 200 KHz were applied in an adjacent injection protocol. The resulting voltage differences were measured by the remaining

electrode pairs after each current injection. The GREIT reconstruction algorithm [19] was used to reconstruct the images.

2.2. Breath detection

In the following, the description of the three proposed algorithms and their related parameters are given. Subsequently, the definition of the gold standard, the optimization and the validation of the methods are presented.

2.2.1 Zero-crossing algorithm

The zero-crossing (ZC) algorithm constantly monitors the time instances of zero crossings in the breath impedance signal and operates with the two states “Wait for Raising Crossing” (WRC) and “Wait for Falling Crossing” (WFC), see Figure 1. The “Identical Crossing Spacings” (ICS) and “Different Crossing Spacings” (DCS) in the breath signal are defined as the differences in the time of consecutive zero crossings with identical or different slopes, respectively. To mitigate the detection of rapid oscillations as being breaths, two threshold parameters are defined, the Minimum Identical Crossing Spacing (MICS) and the Minimum Different Crossing Spacing (MDCS) in seconds. These parameters are also normalized to the maximal breath period so that

$$\begin{aligned} \text{MICS} &= \text{MICSfact} \cdot 60/\text{maxBR} \\ \text{MDCS} &= \text{MDCSfact} \cdot 60/\text{maxBR} \end{aligned} \quad (1)$$

where MICSfact and MDCSfact are the normalized parameters and maxBR the assumed maximal breath rate in breaths/min.

During the WRC state, the algorithm is constantly updating the current minimum of the signal. If a raising zero crossing is detected and both criteria $\text{ICS} > \text{MICS}$ and $\text{DCS} > \text{MDCS}$ are satisfied, then the last minimum is confirmed as the last expiration phase and the state of the algorithm is

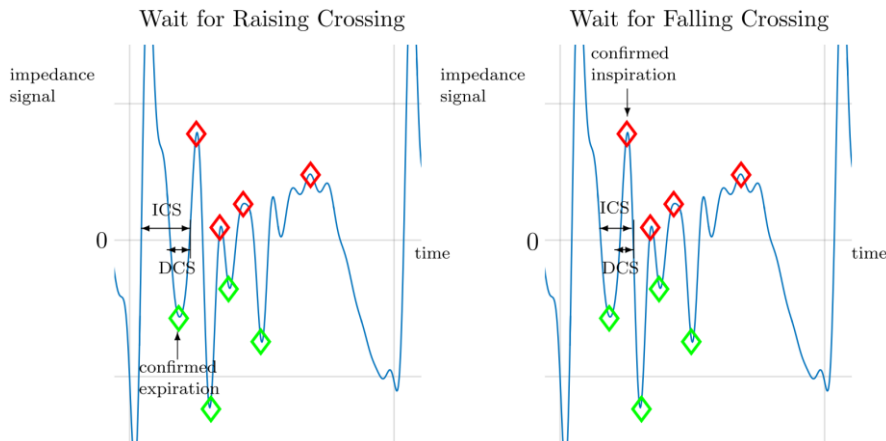


Figure 1. Illustration of the zero-crossing algorithm with Identical Crossing Spacing (ICS) and Different Crossing Spacing (DCS) indicated in the breath (impedance) signal. The green and red diamonds indicate the detected minima and maxima during the expiration and inspiration phases, respectively. Left: end of WRC state and confirmed expiration phase. Right: end of WFC state and confirmed inspiration phase.

changed to WFC. Similarly, during the WFC state, the algorithm is constantly updating the current maximum of the signal. If a falling zero crossing is detected and both criteria $ICS > MICS$ and $DCS > MDCS$ are satisfied, then the last maximum is confirmed as the last inspiration phase and the state of the algorithm is changed to WRC.

Tidal amplitudes are defined as the differences in signal impedance amplitudes between the maxima during the inspiration phases and the corresponding minima during the expiration phases. Here, it is assumed that the expiration phase precedes the inspiration phase during one breathing cycle. With the ZC algorithm, the maximal breath rate parameter is set to $\max BR = 150$ breaths/min and the parameters $MICS_{fact}$ and $MDCS_{fact}$ are optimized as described below.

2.2.2 Zero-crossing algorithm with amplitude threshold

To decrease the rate of False Positives (FP) in breath detections due to superimposed small amplitude changes, such as cardiac related impulses during short periods of no breathing or other disturbances, we propose using an amplitude threshold which has proven to be very efficient. A statistical based threshold is therefore used here as follows. It is assumed that a finite record of data is going to be analyzed where the majority of signal samples (at least more than, e.g., 50%) come from the measurement periods containing breathing signals and not only noise.

To determine a typical value representing large tidal amplitudes, we choose the tidal amplitude $typTA$ at a certain upper percentile UP of all tidal amplitudes in the record. This is to avoid comparing to some large impulsive disturbances, noise or other signal artifacts during the recording. In this study the value $UP = 0.8$ has emerged as a good compromise and has been fixed during the optimization. A lower threshold for tidal amplitudes is then determined as $lowTA = typTA \cdot lowTA_{fact}$ where $lowTA_{fact}$ is a lower amplitude factor chosen in the range $0 < lowTA_{fact} < 1$. In the breath detection algorithm, whenever a tidal amplitude detected by the zero crossing algorithm has a tidal amplitude lower than $lowTA$, it will be discarded as a tidal amplitude and not counted as a breath. With the ZC-AT algorithm, the maximal breath rate parameter is set to $\max BR = 150$ breaths/min, the upper percentile $UP = 0.8$ and the parameters $MICS_{fact}$, $MDCS_{fact}$ and $lowTA_{fact}$ are optimized as described below.

2.2.3 Zero-crossing algorithm with amplitude threshold and FFT-based breath rate estimation

A Short-Time Fourier Transform (STFT) is straightforward to implement on the breath impedance signal $x(n)$ which is given by the sum of pixel (impedance) values obtained from EIT - see details in [19]. The STFT is given here by the following Fast Fourier Transform (FFT) calculation [26] at discrete frequency and time (k, n)

$$X(k, n) = \sum_{l=0}^{M-1} h_l (x_{n-l} - \bar{x}_n) e^{-i \frac{2\pi}{N} kl} . \quad (2)$$

Here, a sliding time window is employed where x_{n-l} denotes the finite sequence of temporary data to be analyzed, h_l the corresponding window weight function of length M , N the size of the FFT,

and where the discrete impedance signal $x(n)$ has been sampled at the frame rate f_s . The mean \bar{x}_n

$$\text{is calculated as } \bar{x}_n = \frac{1}{M} \sum_{l=0}^{M-1} x_{n-l}.$$

A crucial step of any STFT implementation is to determine a suitable trade-off between the resolution in time and frequency. Based on the available set of patient data, we have found that a suitable time window for analysis in our application is about 3 seconds in duration yielding a window length of 143 samples at a frame rate of 48 Hz. A zero padding is used with the parameter $N = 1024$ yielding a FFT frequency resolution of 2.8 breaths/min. A Kaiser window [26-28] is employed to achieve an optimal trade-off between the width of the main-lobe (actual frequency resolution) and the side-lobe rejection in the frequency domain. Here, the Kaiser window was chosen with a main-lobe width of about 30 breaths/min and a side-lobe rejection better than 30 dB. Finally, the breath rate estimate $BR(n)$ is obtained as the breath rate for which the STFT $|X(k, n)|$ has its maximum at time n , see Figure 2.

Note that in (2), it is necessary to subtract the mean \bar{x}_n of the temporary data vector to avoid spectral leakage from the zero frequency component (DC level) in the FFT. However, a further improvement is also obtained by pre-processing the data using a digital high-pass filter to remove the dominating low frequency contents. Here, a second order high-pass Butterworth filter has been used with a cut-off frequency of 15 breaths/min.

A breath alarm level BA is defined in breaths/min. In the breath detection algorithm, whenever a

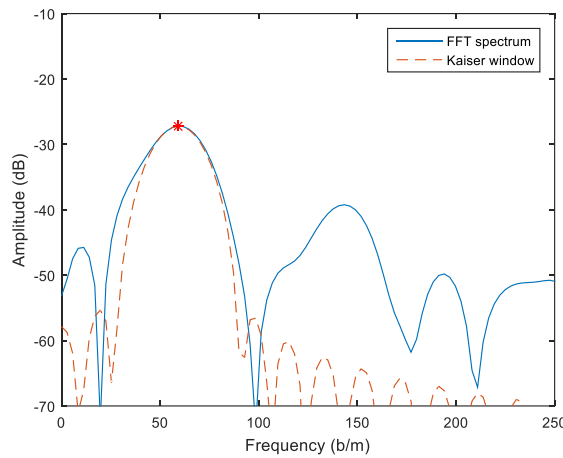


Figure 2. STFT spectrum of the EIT data (blue line) and Kaiser window (dashed line). The respiratory rate estimate is defined as the frequency for which the STFT has its maximum (red star).

tidal amplitude detected by the zero-crossing algorithm has a tidal amplitude lower than $lowTA$, or the estimated breath rate $BR(n)$ is lower than the alarm level BA, it will be discarded as a tidal amplitude and not counted as a breath.

With the ZC-AT-FFT algorithm, the maximal breath rate parameter $maxBR$ is dynamically set to $maxBR(n) = 4 \cdot BR(n)$ breaths/min, the upper percentile $UP = 0.8$ and the parameters $MICSfact$, $MDCSfact$, $lowTAfact$ and BA are optimized as described below.

2.3 Optimization and validation of breath detection

In order to perform an optimization and validation of the breath detection algorithms, there is a need for a gold standard. In the following, details of defining the gold standard and the procedure of optimization and validation will be described.

2.3.1 Gold standard for breath detection

To optimize and validate the breath detection algorithms two sets of data were selected, a test set and a validation set, each set comprising 10 records of CRADL patients' data (impedance signals) with a duration of 80 seconds each.

Based on their experiences as neonatologists working with EIT, 11 clinicians were asked to examine the corresponding impedance plots and to indicate which peaks that correspond to a regular breath cycle, and ignore other peaks. The 80% limit of agreement was defined as a gold standard. It was therefore decided to define as a true breath (or positive breath) all peaks that at least 80% of the clinicians agreed it was a breath, and to mark the other peaks as no breath (or negative breath). The result of the examination (gold standard for breath detection) is illustrated in the Figures 5-6 showing an example of the breath impedance signals together with a red and a black asterisk for a positive and a negative breath, respectively.

2.3.2 Optimization

The test data sets have been used for training in order to optimize the breath detection algorithms ZC, ZC-AT and ZC-AT-FFT, in terms of their Receiver Operating Characteristics (ROC) defined by the corresponding true positive rate (TPR) and false positive rate (FPR) [29]. The validation data sets have then been used to validate the results in terms of the ROC. The number of True Positives (TP), False Negatives (FN), False Positives (FP) and True Negatives (TN) are readily calculated based on the output of each detector in comparison to the gold standard. The TPR and FPR are then calculated based on all the 10 data sets in either the test set or the validation set, respectively.

To define a practical optimization problem in view of the multi-criteria ROC plot, we employ the weighted norm (a weighted metric distance from the optimal point (FPR, TPR) = (0, 1))

$$d(\theta) = \sqrt{w^2 (FPR - 0)^2 + (TPR - 1)^2}, \quad (3)$$

where θ is the parameter vector (e.g., $\theta = (\text{MICSfact}, \text{MDCSfact}, \text{lowTAfact}, \text{BA})$ for the ZC-AT-FFT algorithm), FPR and TPR are the false and true positive rates obtained with the current parameters, and w is a positive weighting factor. The purpose of the weighting is to parameterize the trade-off between the conflicting requirements to have a large TPR (high sensitivity) and a small FPR (high specificity) at the same time. In particular, in our example, we are mostly concerned with emphasizing a small FPR, and a suitable weight for this purpose was found to be $w = 10$.

The discrete nature of this global optimization problem makes the problem very complex. In particular, the parameters of the algorithms are not independent and the change of one parameter may be compensated by a change of another parameter making the solution non-unique. Since the

corresponding global optimization problem becomes huge when increasing the number of degrees of freedom, a practical approach is to use the optimization software to make experiments and to find a good compromise regarding which parameters that realistically can be fixed and which parameters that need to be optimized. In this sense, the resulting parameters will always be suboptimal. The results presented below constitute one such compromise and serves the purpose to illustrate the proposed optimization methods and to quantify the (suboptimal) performances of the breath detectors that have been studied.

To this end, the most important parameter of the detectors ZC-AT and ZC-AT-FFT is the lower amplitude factor lowTAfact for which it was easy to find an optimal interior solution with $0 < \text{lowTAfact} < 1$.

3. Results

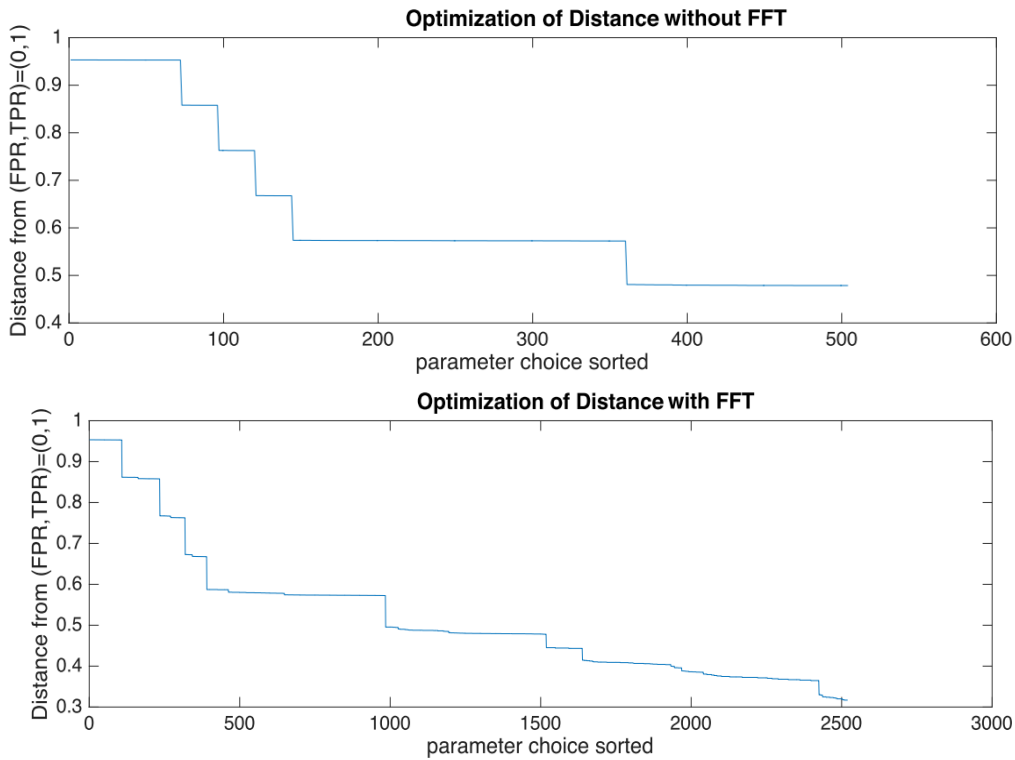


Figure 3. Weighted metrics over the chosen parameter set in the optimization of the ZC-AT and the ZC-AT-FFT algorithms, respectively.

As it is explained in section 2, the proposed metric distance function (3) with a weight $w = 10$ is used to optimize ZC, ZC-AT and ZC-AT-FFT algorithms. Figure 3 shows an example of choosing the optimal parameters based on defining a minimum distance from the perfect optimal point ($\text{TPR} = 1$, $\text{FPR} = 0$). The corresponding metric distances for each possible choice of the parameters are calculated, and shown (sorted) in Figure 3. Figure 4 shows a typical example of determining an optimal lowTAfact when the other parameters are fixed on their optimal values. The search for the optimal lowTAfact has been done in the range of $[0 \ 0.3]$ with the step forward

of 0.001 when MICSfact, MDCSfact and BA are fixed on 0.3, 0.1 and 30, respectively. The most important optimization parameter is lowTAfact where an interior solution satisfying strict bounds $0 < \text{lowTAfact} < 1$ could readily be found. With the other parameters, due to their inherent redundancy, the optimal solution always saturated at the given upper or lower parameter bounds. Hence, considering the discrete nature of this global optimization problem, a relatively small parameter space has been used together with an exhaustive search for minimizing the metric distance function (3) with weight $w = 10$. The following results have been obtained:

- Zero-crossing (ZC) algorithm.

Default parameters: MICSfact=0.75 and MDCSfact=0.25.

Validated performance: FPR=0.23, TPR=0.96.

- Zero-crossing (ZC) algorithm.

Parameter range: $0.5 \leq \text{MICSfact} \leq 0.75$ and $0.1 \leq \text{MDCSfact} \leq 0.25$.

Optimized parameters: MICSfact=0.5 and MDCSfact=0.1.

Validated performance: FPR=0.23, TPR=0.97.

- Zero-crossing algorithm with amplitude threshold (ZC-AT).

Parameter range: $0.5 \leq \text{MICSfact} \leq 0.75$, $0.1 \leq \text{MDCSfact} \leq 0.25$ and $0.1 \leq \text{lowTAfact} \leq 0.3$.

Optimal parameters: MICSfact=0.5, MDCSfact=0.1 and lowTAfact = 0.25.

Validated performance: FPR=0.08, TPR=0.95.

- Zero-crossing algorithm with amplitude threshold and FFT-based breath-rate estimation (ZC-TA-FFT).

Parameter range: $0.5 \leq \text{MICSfact} \leq 0.75$, $0.1 \leq \text{MDCSfact} \leq 0.25$,

$0.1 \leq \text{lowTAfact} \leq 0.3$ and $0 \leq \text{BA} \leq 40$.

Optimal parameters: MICSfact=0.5, MDCSfact=0.25, lowTAfact = 0.15 and BA = 30.

Validated performance: FPR=0.06, TPR= 0.84.

Figure 5 shows a result of using the ZC-AT algorithm with optimal parameters for a typical breath detection example using the validation data set. The upper plot shows the breath impedance signals together with a red and a black asterisk for a positive and a negative breath, respectively. A four seconds interval at the beginning and at the end of each data have been excluded from the investigation, allowing the breath detectors to stabilize and avoid edge effects. The lower plot shows the output of the optimized ZC-AT detector. The performance in terms of TP, FN, FP and TN is shown in the title of the upper plot. It is seen that the ZC-AT algorithm performs with 36 TPs and 3 FPs (indicated in the figure).

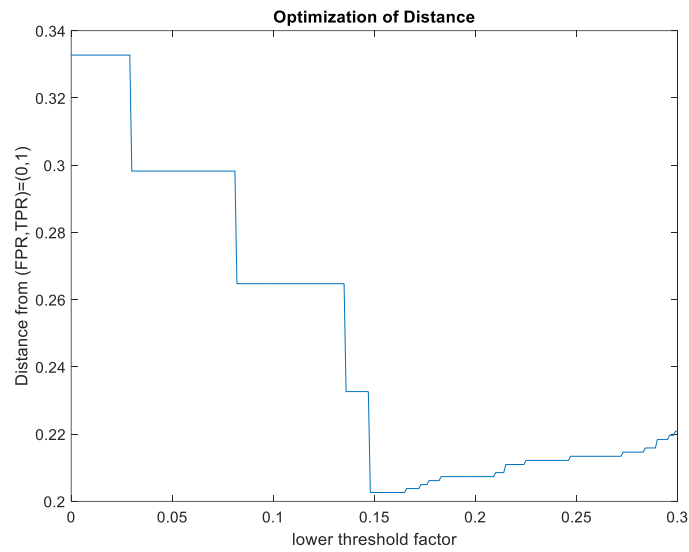


Figure 4. A typical example of determining an optimal lowTAfact when the other parameters fixed on their optimal values.

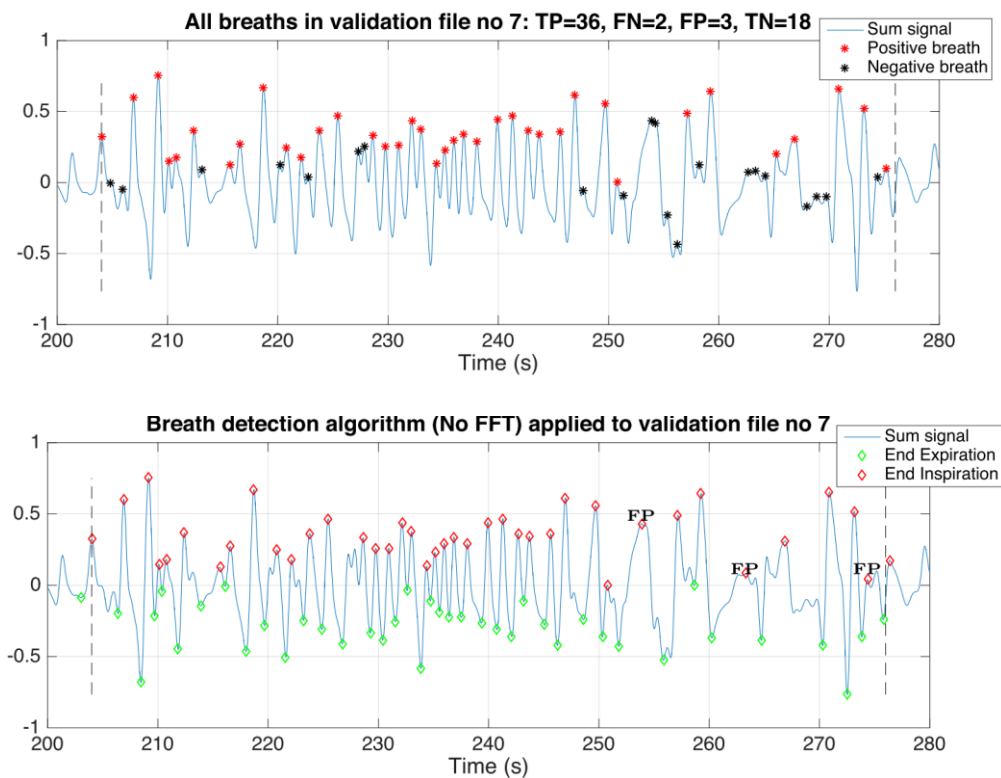


Figure 5. Breath detection performance on the validation data no.7 with zero-crossing algorithm complemented with amplitude threshold (ZC-AT).

In Figure 6 the ZC-AT-FFT algorithm with optimal parameters is used for the same particular breaths as in Figure 5. The second and third plots show the output of the optimized detector using the ZC-AT-FFT algorithm and the corresponding estimated breath rate, respectively. The detector performs with 1 FP and 29 TPs for the same data. It is easy to identify the particular breaths where the ZC-AT-FFT algorithm is able to avoid 2 of the FPs by employing a breath alarm level (BA). However, this is done with the cost of neglecting TPs in the area/situations with breath rate lower than BA.

The results for both test and validation data are illustrated in the corresponding Receiver Operating Characteristics (ROC) plots shown in Figure 7. The upper plot shows the results with the ZC-AT-FFT algorithm and the lower plot with the ZC-AT algorithm. The green circles indicate the performances obtained with the various parameter settings calculated over the 10 testing (training) data, the red asterisk indicates the optimal point over the test set and the blue asterisk indicates the corresponding performance calculated over the validation set. The black asterisk and the black circle indicate the validated performance of the ZC algorithm, with default parameters and optimal parameters as described above, respectively. It is seen that both the ZC-AT-FFT and the ZC-AT algorithms performs better than both the default ZC and the optimized ZC algorithm in test and validation data set. With the current weight ($w=10$), the ZC-AT-FFT results in slightly lower FPR than the ZC-AT whereas, the ZC-AT provide slightly higher TPR than the ZC-AT-FFT algorithm.

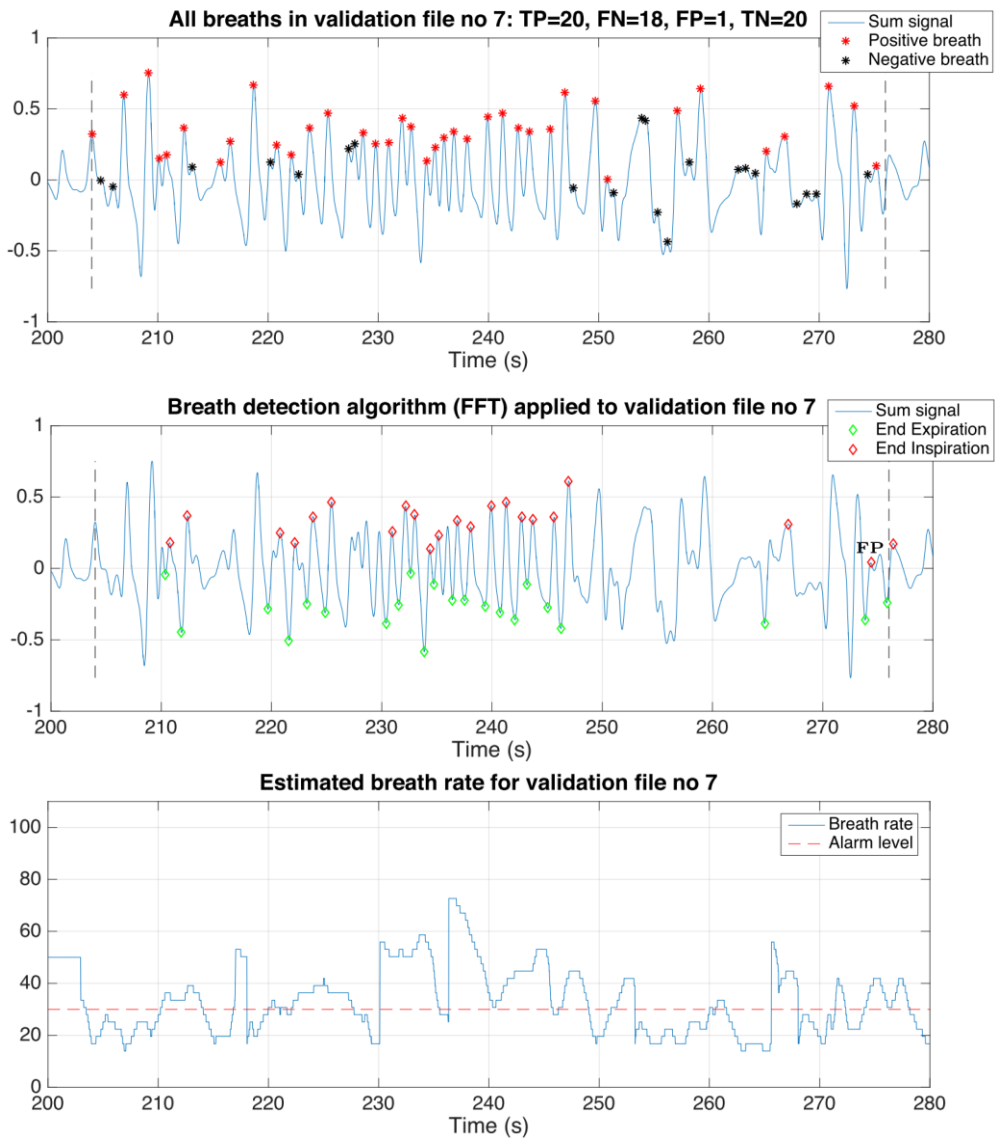


Figure 6. Breath detection performance on the validation data no.7 with zero-crossing algorithm complemented with amplitude threshold and FFT-based breath-rate estimation (ZC-AT-FFT).

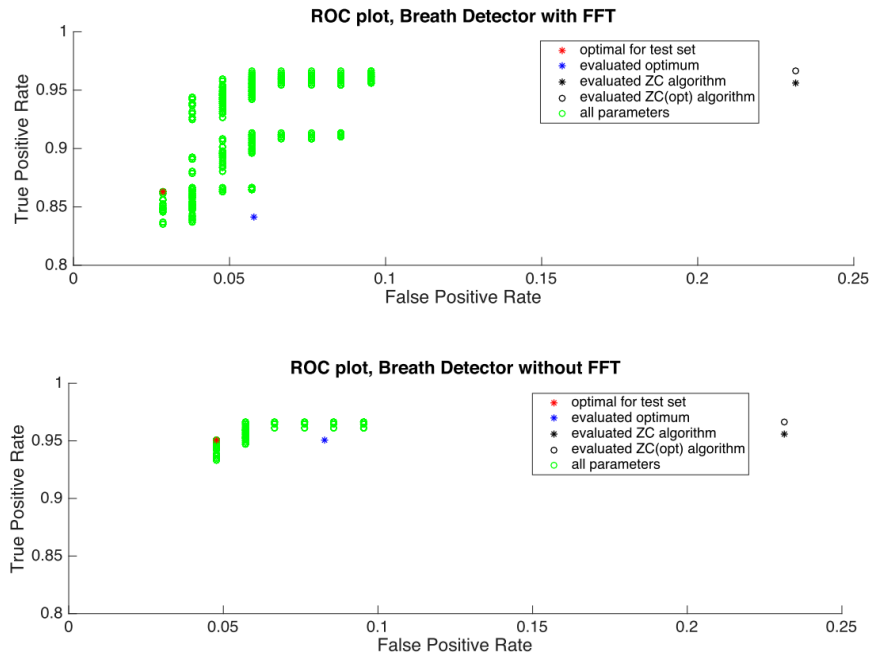


Figure 7: Receiver Operation Characteristics (ROC) for breath detection with the ZC-AT-FFT (upper plot) and ZC-AT (lower plot) algorithms, and a comparison with the ZC algorithm.

5. Summary and conclusions

A generic framework for optimizing the breath delineation algorithms used in Electrical Impedance Tomography has been given in this paper. In particular, the approach is based on the definition of a gold standard for breath detection, the associated sensitivity and specificity measures, an adequate optimization criterion defined on the ROC-plane and a set of detector parameters to be optimized.

The results show that both the ZC-AT and the ZC-AT-FFT algorithms outperform the conventional ZC algorithm in terms of the ROC. The main reason for this is that the amplitude threshold is able to avoid small amplitude disturbances (such as cardiac related signal components, etc) during periods of little or no breathing being interpreted as breaths. The addition of the FFT-based breath rate estimate is able to further decrease the FPR, but only at the expense of a decreased sensitivity. The ZC-AT-FFT algorithm has the advantage to output the auxiliary instantaneous, short-time estimate of the breath rate. Its disadvantage, however, is the higher computational complexity (of the short-time FFT) as compared to the ZC-AT algorithm.

Acknowledgments

We acknowledge the grants from the European Union's Framework program for research and innovation Horizon 2020 (CRADL, Grant No. 668259). **Switzerland government??**

References

1. Schmidt, M., et al., *Comparative investigations of algorithms for the detection of breaths in newborns with disturbed respiratory signals*. Comput. Biomed. Res., 1998. **31**(6): p. 413-425.
2. Bates, J., et al., *Tidal breath analysis for infant pulmonary function testing*. ERS/ATS Task Force on Standards for Infant Respiratory Function Testing. European Respiratory Society/American Thoracic Society. European Respiratory Journal, 2000. **16**(6): p. 1180-1192.
3. Govindarajan, N. and O. Prakash, *Breath detection algorithm in digital computers*. International journal of clinical monitoring and computing, 1990. **7**(1): p. 59-64.
4. Nguyen, C.D., et al., *An automated and reliable method for breath detection during variable mask pressures in awake and sleeping humans*. PLOS ONE, 2017. **12**(6): p. e0179030.
5. Ruinskiy, D. and Y. Lavner, *An Effective Algorithm for Automatic Detection and Exact Demarcation of Breath Sounds in Speech and Song Signals*. IEEE Transactions on Audio, Speech, and Language Processing, 2007. **15**(3): p. 838-850.
6. de Waal, C.G., et al., *Breath detection by transcutaneous electromyography of the diaphragm and the Graseby capsule in preterm infants*. Pediatric Pulmonology, 2017. **52**(12): p. 1578-1582.
7. Kraaijenga, J.V., et al., *Transcutaneous electromyography of the diaphragm: A cardio-respiratory monitor for preterm infants*. Pediatric pulmonology, 2015. **50**(9): p. 889-895.
8. Carlisle, H.R., et al., *Regional distribution of blood volume within the preterm infant thorax during synchronised mechanical ventilation*. Intensive Care Medicine, 2010. **36**.
9. Dunlop, S., et al., *Electrical impedance tomography in extremely prematurely born infants and during high frequency oscillatory ventilation analyzed in the frequency domain*. Physiological Measurement, 2006. **27**.
10. Frerichs, I., et al., *Chest electrical impedance tomography examination, data analysis, terminology, clinical use and recommendations: consensus statement of the TRanslational EIT developmeNt stuDy group*. Thorax, 2016.
11. Chatziioannidis, I., et al., *Assessment of lung ventilation in infants with respiratory distress syndrome using electrical impedance tomography*. Hippokratia, 2013. **17**(2): p. 115-119.
12. de Souza Rossi, F., et al., *Electrical impedance tomography to evaluate air distribution prior to extubation in very-low-birth-weight infants: a feasibility study*. Clinics, 2013. **68**(3): p. 345-350.
13. Durlak, W. and P. Kwinta, *Role of Electrical Impedance Tomography in Clinical Practice in Pediatric Respiratory Medicine*. ISRN Pediatrics, 2013. **2013**: p. 5.
14. Chatziioannidis, I., T. Samaras, and N. Nikolaidis, *Electrical Impedance Tomography: a new study method for neonatal Respiratory Distress Syndrome?* Hippokratia, 2011. **15**(3): p. 211-215.
15. Brown, B.H., D.C. Barber, and A.D. Seagar, *Applied potential tomography: Possible clinical applications*. Clinical Physics and Physiological Measurement, 1985. **6**(2): p. 109-121.
16. Kerrouche, N., C. McLeod, and W. Lionheart, *Time series of EIT chest images using singular value decomposition and Fourier transform*. Physiological Measurement, 2001. **22**(1): p. 147.

17. Deibele, J.M., H. Luepschen, and S. Leonhardt, *Dynamic separation of pulmonary and cardiac changes in electrical impedance tomography*. Physiological Measurement, 2008. **29**.
18. Grant, C.A., et al., *Measurement of ventilation and cardiac related impedance changes with electrical impedance tomography*. Critical Care, 2011. **15**(1): p. R37.
19. Adler, A., et al., *GREIT: a unified approach to 2D linear EIT reconstruction of lung images*. Physiol Meas, 2009. **30**(6): p. S35-55.
20. Li, C., D.F. Parham, and Y. Ding. *Cycle detection in speech breathing signals*. in *Proceedings of the 2011 Biomedical Sciences and Engineering Conference: Image Informatics and Analytics in Biomedicine*. 2011.
21. Zadehkoochak, M., et al., *Pulmonary perfusion and ventricular ejection imaging by frequency domain filtering of EIT images*. Clinical Physics and Physiological Measurement, 1992. **13**(A): p. 191.
22. Marven, S.S., et al., *Reproducibility of electrical impedance tomographic spectroscopy (EITS) parametric images of neonatal lungs*. Physiological Measurement, 1996. **17**(4A): p. A205.
23. Rahman, T., et al., *Extraction of cardiac and respiration signals in electrical impedance tomography based on independent component analysis*. Journal of Electrical Bioimpedance, 2013. **4**(1): p. 38-44.
24. Khodadad, D., et al. *Breath detection using short-time Fourier transform analysis in Electrical Impedance Tomography*. in *32nd International Union of Radio Science General Assembly & Scientific Symposium*. 19 - 23 Aug, 2017. Montreal, QC, Canada: 32nd URSI GASS.
25. S. Nordebo, M.D., D. Khodadad, B. Muller, A. Waldman, T. Becher, I. Frerichs, L. Sophocleous, and N.S. D. Sjöberg, Richard Bayford, *A parametric model for the changes in the complex valued conductivity of a lung during tidal breathing*. Submitted to J. Phys. D: Appl. Phys., 2017. (**arXiv version**).
26. Oppenheim, A.V., *Discrete-Time Signal Processing*. 1999: Pearson Education.
27. Kaiser, J.F. *Nonrecursive digital filter design using the I_0 -sinh window function*. in *Proc. IEEE Int. Symp. Circuits & Syst.*, 1974. 1974.
28. Kaiser, J. and R. Schafer, *On the use of the I_0 -sinh window for spectrum analysis*. IEEE Transactions on Acoustics, Speech, and Signal Processing, 1980. **28**(1): p. 105-107.
29. Beck, J.R. and E.K. Shultz, *The use of relative operating characteristic (ROC) curves in test performance evaluation*. Archives of pathology & laboratory medicine, 1986. **110**(1): p. 13-20.